

Crystal-phase engineering of PdCu nanoalloys facilitates selective hydrodeoxygenation at room temperature

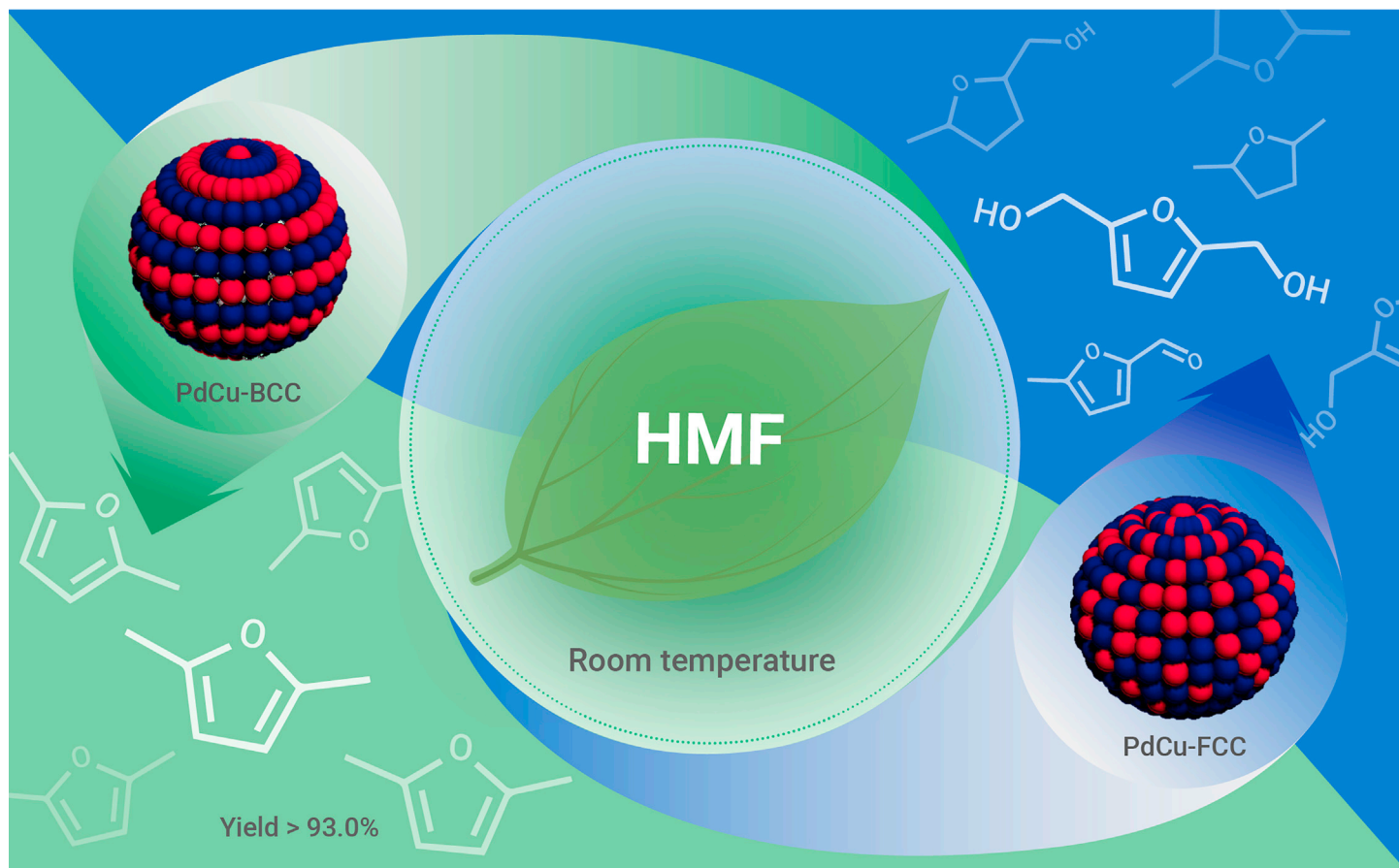
Shaopeng Li,^{1,5} Minghua Dong,^{1,2,5} Mi Peng,^{3,5} Qingqing Mei,¹ Yanyan Wang,^{1,2} Junjuan Yang,¹ Youdi Yang,¹ Bingfeng Chen,¹ Shulin Liu,^{1,2} Dequan Xiao,⁴ Huizhen Liu,^{1,2,*} Ding Ma,^{3,*} and Buxing Han^{1,2,*}

*Correspondence: liuhz@iccas.ac.cn (H.L.); dma@pku.edu.cn (D.M.); hanbx@iccas.ac.cn (B.H.)

Received: February 2, 2021; Accepted: November 23, 2021; Published Online: November 26, 2021; <https://doi.org/10.1016/j.xinn.2021.100189>

© 2021 The Authors. This is an open access article under the CC BY-NC-ND license (<http://creativecommons.org/licenses/by-nc-nd/4.0/>).

Graphical abstract



Public summary

- Selectively cleaving of C–O bonds in lignocellulosic biomass is very difficult. The PdCu nanoalloys can catalyze the selective hydrodeoxygenation reaction of HMF to DMF
- The PdCu nanoalloys with specific crystallographic phases can improve the selectivity of hydrodeoxygenation reaction
- The body-centered cubic (BCC) PdCu nanoalloys exhibited outstanding performance with 93.6% yield of DMF at room temperature
- PdCu/AC-BCC could also catalyze other aromatic alcohols at room temperature



Crystal-phase engineering of PdCu nanoalloys facilitates selective hydrodeoxygenation at room temperature

Shaopeng Li,^{1,5} Minghua Dong,^{1,2,5} Mi Peng,^{3,5} Qingqing Mei,¹ Yanyan Wang,^{1,2} Junjuan Yang,¹ Youdi Yang,¹ Bingfeng Chen,¹ Shulin Liu,^{1,2} Dequan Xiao,⁴ Huizhen Liu,^{1,2,*} Ding Ma,^{3,*} and Buxing Han^{1,2,*}

¹Beijing National Laboratory for Molecular Sciences, Key Laboratory of Colloid and Interface and Thermodynamics, CAS Research/Education Center for Excellence in Molecular Sciences, Institute of Chemistry, Chinese Academy of Sciences, Beijing 100190, China

²School of Chemical Science, University of Chinese Academy of Sciences, Beijing 100049, China

³Beijing National Laboratory for Molecular Engineering, College of Chemistry and Molecular Engineering and College of Engineering, BIC-ESAT, Peking University, Beijing 100871, China

⁴Center for Integrative Materials Discovery, Department of Chemistry and Chemical Engineering, University of New Haven, West Haven, CT 06516, USA

⁵These authors contributed equally

*Correspondence: liuhz@iccas.ac.cn (H.L.); dma@pku.edu.cn (D.M.); hanbx@iccas.ac.cn (B.H.)

Received: February 2, 2021; Accepted: November 23, 2021; Published Online: November 26, 2021; <https://doi.org/10.1016/j.xinn.2021.100189>

© 2021 The Authors. This is an open access article under the CC BY-NC-ND license (<http://creativecommons.org/licenses/by-nc-nd/4.0/>).

Citation: Li S., Dong M., Peng M., et al., (2022). Crystal-phase engineering of PdCu nanoalloys facilitates selective hydrodeoxygenation at room temperature. *The Innovation* **3**(1), 100189.

Selective hydrodeoxygenation of biomass-derived aromatic alcohols to value-added chemical or fuel is of great importance for sustainable biomass upgrading, and hydrodeoxygenation of 5-hydroxymethylfurfural (HMF) to 2,5-dimethylfuran (DMF) is one of the most attractive reactions. Achieving the conversion of HMF to DMF using H₂ at ambient temperature is challenging. In this work, we used PdCu nanoalloys to catalyze the selective hydrodeoxygenation reaction of HMF to DMF using H₂ as the reducing agent. The reaction path and the product selectivity are governed by the crystallographic phase of the PdCu nanoalloys. It was discovered that body-centered cubic (BCC) PdCu nanoalloys supported on activated carbon (AC) exhibited outstanding performance with 93.6% yield of DMF at room temperature (PdCu/AC-BCC). A combination of experimental and density functional theory (DFT) studies showed that the tilted adsorption modes of furanic intermediates on PdCu-BCC nanoalloy surfaces accounted for the high selectivity of DMF; however, furan ring was activated on PdCu face-centered cubic (FCC) nanoalloy surfaces. Furthermore, PdCu/AC-BCC could also catalyze the hydrodeoxygenation of other aromatic alcohols at room temperature while maintaining the aromatic structures. This work opens the way for selective hydrodeoxygenation of the aromatic alcohols at room temperature with the aromatic ring intact.

INTRODUCTION

Production of commodity chemicals from renewable feedstocks has received significant attention as a promising way to diminish our dependence on fossil resources and construct sustainable chemical industries.^{1–6} Transition-metal-catalyzed hydrodeoxygenation reaction of oxygenated organic compounds has attracted broad interest in recent years because of their important role in biomass feedstock transformation as well as in pharmaceuticals industry. However, selectively activating and cleaving C–O bonds in lignocellulosic biomass is very difficult. On the one hand, the commonly used noble metal catalysts often have strong hydrogenation ability to C=C bonds and aromatic rings, which are ubiquitous in biomass-derived compounds, resulting in undesirable product. On the other hand, in order to obtain high conversion and product selectivity, a high reaction temperature is often required.

The selective hydrodeoxygenation of 5-hydroxymethylfurfural (HMF), which is considered an important biomass platform chemical, to 2,5-dimethylfuran (DMF) is one of the most attractive reactions in biomass transformation. DMF has been identified as a highly interesting candidate of liquid fuel with high energy densities (30 kJ·cm⁻³) and research octane numbers (RON = 119), holding great potential to substitute for petroleum-based gasoline, and can also be converted to valuable benzene-based chemicals via Diels-Alder reactions.^{7–11} Various products, such as 2,5-bis(hydroxymethyl)furan (DHMF), 5-methylfurfural (5-MF), 5-methylfurfuralalcohol (5-MFA), 2,5-bis(hydroxymethyl)tetrahydrofuran (DHTHF), 5-methyltetrahydrofuran-2-methanol (MTHFM), 2-hexanol (HOL), and 2,5-dimethyltetrahydrofuran (DMTHF), are produced in the catalytic HMF hydrodeoxygenation reaction as side products, as shown in [Scheme S1](#). Indeed, different catalytic systems have been used for selective hydrodeoxygenation of HMF to DMF.¹² Bimetallic catalytic systems play an important role in improving DMF selectivity by forming core-shell structure, electronic effect between two metals, and providing multiple sites.^{13–16} Pt₃Co₂ nanoparticles were used in transformation of HMF to

DMF with 98% yield at 160°C, and it was modeled as an alloy core covered by a Co₃O₂ monolayer, in which the Co₃O₂ layer repelled furan rings to prevent further hydrogenation.¹⁷ Similar to Pt₃Co₂ core-shell structures, near-ambient-pressure X-ray photoelectron spectroscopy (NAP-XPS) suggested that NiCu₃ nanocrystals involve a Cu-rich core and a 1:1 molar Ni:Cu shell, which exhibited a DMF yield of 98.7% at 180°C.¹⁴ One-hundred percent HMF conversion and 92.9% selectivity to DMF were obtained over Co-alloyed Pt single-atom catalysts under 1.0 MPa H₂ at 180°C, where Pt sites were responsible for H₂ activation and Pt^{δ-}–Co^{δ+} sites activated C–O bonds.¹⁶ Cobalt and copper bimetallic catalyst on N-graphene-modified Al₂O₃ could efficiently catalyze the selective hydrodeoxygenation of HMF to DMF at 180°C, and the catalytic performance resulted from the synergistic effect between defects and active metal.¹⁸ Co@Cu/3CoAlO_x sequentially catalyzed the C=O hydrogenation and C–OH hydrogenolysis to yield as high as 98.5% DMF at 180°C.¹⁹ It is generally accepted that crystallographic phases of nanoalloy catalysts could also affect the catalytic performance. However, synthesizing nanoalloys with specific crystallographic-phase catalysts to improve the selectivity of hydrodeoxygenation reaction of HMF has not yet been reported. More importantly, although satisfactory DMF yield has been obtained over the catalytic systems that have been reported, the harsh reaction conditions required usually cause serious issues and thus limit their practical applications. It is urgent to explore an efficient catalytic system to achieve the conversion of HMF to DMF under mild conditions, especially at room temperature.

Cu–Pd/reduced graphene oxide could catalyze the selective hydrogenation of HMF to DMF using 2-propanol as the reducing agent.²⁰ Hydrogen is an ideal reducing agent. However, when hydrogen was used as the hydrogenation agent, only Pd-based catalysts could catalyze the selective hydrodeoxygenation of HMF to DMF at temperatures lower than 100°C, but the addition of acid as promoter is necessary.²¹ For example, 96% yield of DMF was obtained over PdAu/C catalyst at 60°C in the presence of HCl. In this work, we synthesized PdCu nanoalloys and achieved the selective hydrogenation reaction of HMF to DMF at ambient temperature using H₂ as the reducing agent. It was discovered that the synthesized body-centered cubic (BCC) PdCu nanoalloys supported on activated carbon (AC) (i.e., PdCu/AC-BCC) displayed outstanding performance for hydrodeoxygenation reaction, with a DMF yield of 93.6% at room temperature. The crystallographic phase of PdCu nanoalloys governed the selectivity of the hydrogenation of HMF. The hydrogenation of furan ring was dominating over face-centered cubic (FCC) PdCu nanoalloys supported on AC (PdCu/AC-FCC) with low selectivity toward DMF. Density function theory (DFT) studies showed that the loose arrangement of surface atoms in PdCu-BCC repelled furan rings, while ring adsorptions were favored by close-packing PdCu-FCC surfaces. Moreover, PdCu/AC-BCC could also catalyze the hydrodeoxygenation of other aromatic alcohols at room temperature while maintaining aromatic structures.

RESULTS

The PdCu/AC-BCC catalyst was synthesized by an impregnation-reduction-calcination method, the details of which are shown in the section “[materials and methods](#).” [Figures 1A](#) and [S1](#) show the transmission electron microscopy (TEM) images of the as-prepared PdCu/AC-BCC. Uniform nanoparticles with average diameter of 4.8 nm were immobilized over the AC support. [Figure 1B](#) gives an aberration-corrected high-angle annular dark-field (HAADF) scanning

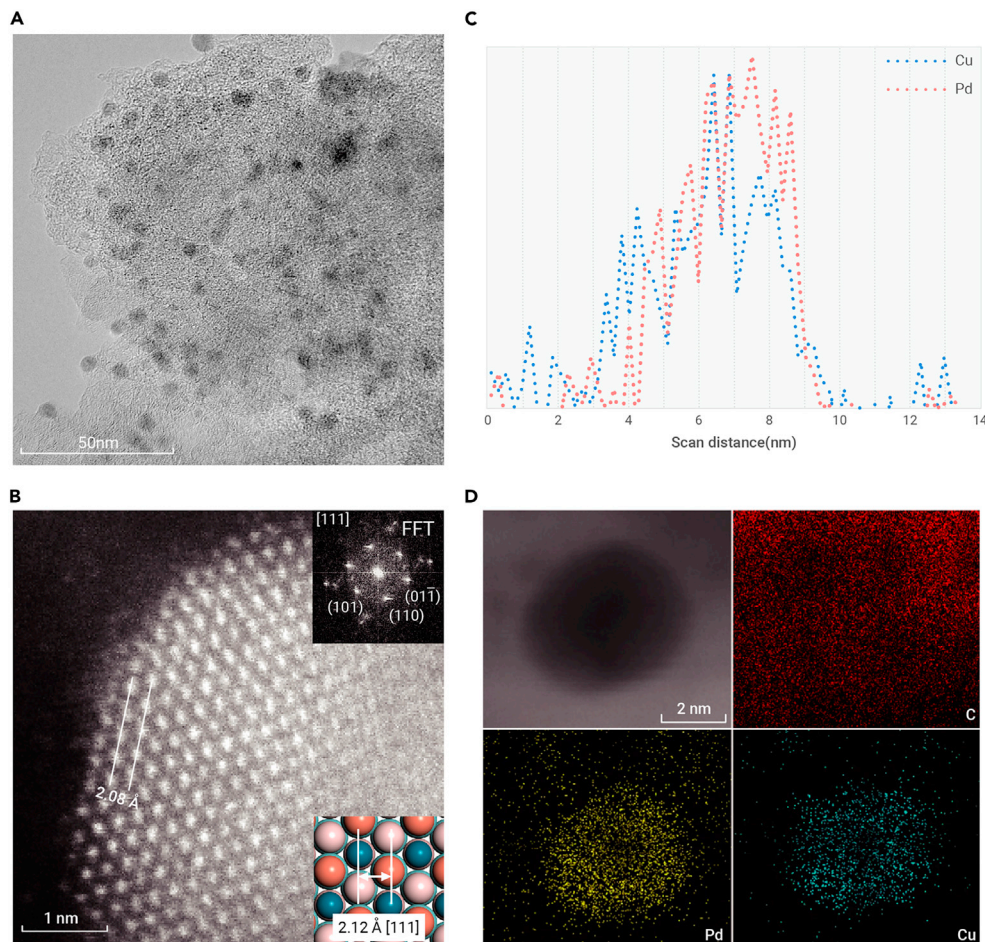


Figure 1. Characterizations of PdCu/AC-BCC catalyst (A) TEM images of PdCu/AC-BCC catalyst. (B) Aberration-corrected HAADF-STEM image of PdCu/AC-BCC; inset: the corresponding fast Fourier transform (FFT) of BCC structure of PdCu along [111] (top); crystal structure of PdCu nanoalloys, top layer Pd and Cu atoms are represented as blue and brown balls (down). (C) STEM line scans of PdCu/AC-BCC. (D) EDS elemental mapping images (Pd, Cu, and C elements) of the PdCu/AC-BCC.

TEM (AC-STEM) image taken from a typical PdCu nanoparticle. The alloy particles have a lattice spacing of 2.08 Å, which is in good agreement with the value of the (111) plane of PdCu-BCC nanoalloys. The STEM line scan results show that the elements of Pd and Cu are homogeneously distributed throughout nanoparticle (Figure 1C), which is confirmed by the corresponding energy dispersive spectroscopy (EDS) elemental mapping images (Figure 1D). Inductively coupled plasma atomic emission spectroscopy (ICP-AES) analysis showed that PdCu/AC-BCC contained 0.54 wt % Pd and 0.31 wt % Cu; i.e., the Pd/Cu atomic ratio was about 1:1. Additional TEM images of PdCu/AC-BCC reveal the uniformity of PdCu nanoalloys (Figure S2). For comparison, FCC-structured PdCu nanoalloys (PdCu/AC-FCC) at an annealing temperature of 200°C were prepared (using the same precursor and composition as that for PdCu/AC-BCC; see section “materials and methods”). Figure S7 gives the HAADF-STEM image taken from a typical individual PdCu nanoparticle in the PdCu/AC-FCC, which demonstrates the formation of nanoalloy with lattice spacing of 1.99 Å, and the result was consistent with the value of (100) plane of PdCu-FCC nanoalloys. Furthermore, the PdCu nanoalloys crystalline structure was also characterized by X-ray diffraction (XRD) and the results are shown in Figure S8. No obvious diffraction peaks of metallic PdCu were observed in the PdCu/AC-FCC and PdCu/AC-BCC catalysts, mainly because of ultra-small size and good dispersion of the nanoalloys. To get more information about the crystal structure, the PdCu nanoalloys without support were prepared and characterized by XRD (Figure S8). The XRD peaks of PdCu nanoalloys without support annealed at 200°C can be indexed as FCC structure. The PdCu-BCC (110) and (100) peaks at 42.9° and 62.2° are clearly visible in Figure S8 for the PdCu nanoalloys annealed at 400°C, suggesting the formation of PdCu-BCC structure. Similarly, the results were obtained on the PdCu/AC 10 wt % indicating that the crystal structure can be tuned by the simple annealing treatment (Figure S9).^{22,23}

The XPS technique was used to study the electronic structure of Pd and Cu components in different catalysts (Figure 2). Compared with Pd/AC, PdCu/AC-BCC showed reduced binding energies for Pd 3d, i.e., 341.0 eV (Pd 3d_{3/2}) and 335.7 eV (Pd 3d_{5/2}), suggesting that Pd was slightly negative charged in PdCu/

AC-BCC (Figure 2A). Likely, Pd receives the electron from Cu in the nanoalloys. The Cu 2p peak exhibits 0.5 eV shift toward higher binding energy in reference to mono-metallic Cu/AC catalyst (Figure 2B), confirming electron transfer from Cu to Pd. Thus, the addition of Cu to Pd results in enrichment of electron density on Pd, showing the strong electron interaction between Pd and Cu. A similar phenomenon was found in the XPS of PdCu/AC-FCC (Figure S10). The valence of Cu was further determined by LMM Auger spectra (Figure S11). Despite the poor signal-to-noise ratio, it can be found that Cu L₃M_{4,5}M_{4,5} peak locates in 918 eV, indicating the existence of metallic Cu compared with reported results.²⁴ The amount of Cl and B in PdCu/AC-BCC were evaluated by ICP mass spectrometry (ICP-MS), both of which were less than 0.01 wt %. Also, XPS showed no residual Cl and B in PdCu/AC-BCC (Figure S12).

The performance of various catalysts for the hydrodeoxygenation of HMF at different temperatures was studied (Table 1). No target product was formed without any catalysts (Table 1, entry

1), and AC was inactive in the reaction (Table 1, entry 2). The activity of AC-supported Pd nanoparticles catalyst (Pd/AC, with a similar Pd loading to that of PdCu/AC-BCC) was very low and the yield of DMF was only 6% at 30°C (Table 1, entry 3). Similarly, AC-supported Cu (Cu/AC) was inactive for the reaction (Table 1, entry 4). To our surprise, a very high DMF selectivity of 93.6% was observed over PdCu/AC-BCC (Table 1, entry 5). These results indicated PdCu/AC-BCC was an outstanding catalyst for hydrodeoxygenation of HMF. The reason for the excellent performance is discussed in the following sections. Interestingly, increasing the reaction temperature to 100°C increased the reaction rate of PdCu/AC-BCC (71.2 h⁻¹; Table 1, entry 6), which is much higher than those in previous reports at similar reaction conditions (Table S1). At 160°C, the yield of DMF could reach 97.2% (Table 1, entry 7), demonstrating that further hydrogenation to the furan ring was still inhibited at high temperature. Moreover, the hydrodeoxygenation of HMF to DMF could be carried out under atmospheric pressure and room temperature over PdCu/AC-BCC, and the yield of DMF reached 38.6% (Table 1, entry 8). These results verified that PdCu/AC-BCC is an excellent catalyst for selective hydrogenation of HMF at low temperature. The effect of H₂ pressure and initial HMF concentration were also checked and the results are shown in Table S4. The conversion and DMF yield increased as hydrogen pressure while decreasing as initial HMF concentration (Table S4, entries 1–5). The catalyst loading also affected the catalytic performance and, when the catalyst loading was 0.5 wt %, the HMF conversion and DMF yield were only 56% and 52%, respectively (Table S4, entries 6 and 7).

Very interestingly, the selectivity of DMF depended strongly on the crystallographic phase of PdCu nanoparticles in the catalysts (Figure 3A and Table S2). The PdCu/AC-BCC catalyzed the hydrodeoxygenation reaction selectively with 93.6% selectivity of DMF. However, the PdCu/AC-FCC promoted the hydrogenation of the furan ring with only 9.0% selectivity to DMF under the same reaction conditions. The effect of reaction time over the PdCu/AC-BCC is shown in Figure 3B. Clearly, for PdCu/AC-BCC, the conversion of HMF increased with the increase of reaction time, reaching a full conversion at around 16 h at 30°C. The selectivity toward DMF of PdCu/AC-BCC increased with the increase of

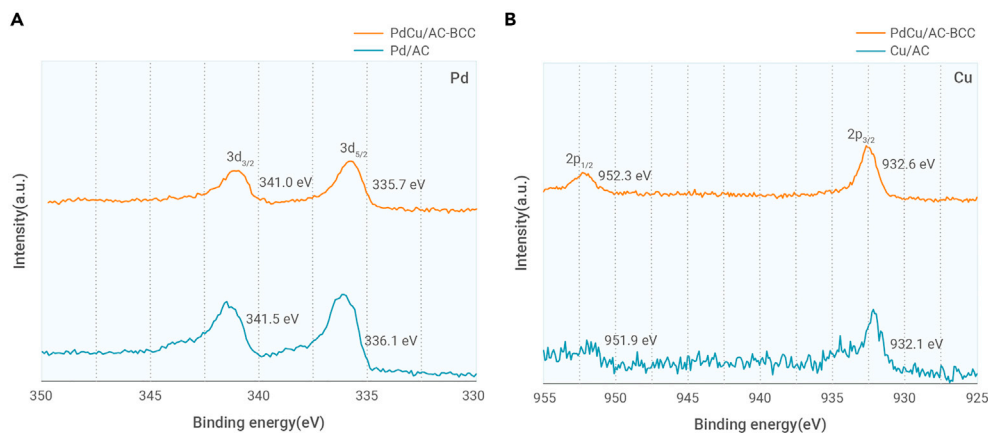


Figure 2. XPS patterns of the catalysts (A) Pd 3d for Pd/AC and PdCu/AC-BCC. (B) Cu 2p for Cu/AC and PdCu/AC-BCC.

reaction time and reached 93.6% after 20 h, because DMF was formed via intermediates. At a reaction of 20 h, besides DMF and trace amounts of other products, only about 5% DHMF was detected. Even after the reaction time was extended to 24 h, DMF was not hydrogenated to DMTHF, demonstrating that PdCu/AC-BCC was capable of selectively catalyzing the designated reaction rather than the deep hydrogenation of furan rings to undesired products. As shown in Table S7, the carbon balances of the reaction at different reaction times were all above 94%.

Different from that of PdCu/AC-BCC catalyst, the main product was DHMF with only 18% yield of the desired product DMF, although the conversion of HMF could reach 99.9% in 4 h over PdCu/AC-FCC (Figure S13). DHMF became the dominant product with the prolonging reaction time, indicating that DHMF was converted to DMTHF. DMF, MTHFM, 5-MFA, and 5-MF were also detected. The yield of DMF decreased to 8% in 24 h and it was further hydrogenated to DMTHF. These results suggested that the reaction pathways over PdCu/AC-FCC include the hydrogenation of the furan ring and the hydrodeoxygenation reaction. Furthermore, the total yield of DHMF and DMTHF was much higher than DMF. Throughout the reaction process, no single product could reach a selectivity higher than 50%, showing that PdCu/AC-FCC is not a highly selective catalyst for the hydrodeoxygenation of HMF. To verify the result for the high selectivity to DMF, control experiments using DMF as the substrate were conducted (Table S3). Notably, under the similar reaction conditions, while DMF was fully converted to DMTHF through the hydrogenation of furan ring over PdCu/AC-FCC, the hydrogenation of DMF was almost completely blocked over PdCu/AC-BCC, confirming that the lattice structure of PdCu is responsible for its selectivity. The support also affected the catalytic performance, and PdCu-BCC and PdCu-FCC are inactive for the reaction (Table S5).

Table 1. Hydrogenolysis of HMF to DMF over various catalysts

Entry	Catalyst	Temperature (°C)	Time (h)	Conversion (%)	Yield (%)	Rate ^a (h ⁻¹)
1	–	30	20	0	0	–
2	AC	30	20	0	0	–
3	Pd/AC	30	20	15	6	–
4	Cu/AC	30	20	trace	–	–
5	PdCu/AC-BCC	30	20	>99	93.6	4.7
6 ^b	PdCu/AC-BCC	100	2	>99	94.3	71.2
7 ^b	PdCu/AC-BCC	160	1	>99	97.2	145.3
8 ^c	PdCu/AC-BCC	30	20	45	38.6	1.6

Reaction conditions: HMF (38 mg); catalyst (30 mg); THF (2 mL); H₂ pressure (4 MPa).

^aRate = moles of product × moles of metal⁻¹ × h⁻¹.

^b20 mg of catalyst.

^cAmbient H₂ pressure.

higher hydrogenation activity than the BCC phase (Table S8).

The DFT calculations were performed to investigate the origin of crystalline-phase-controlled selectivity. According to the literature and AC-STEM results, (100) and (111) surfaces were built to represent the exposed facets of PdCu-FCC and BCC nanoparticles (Figures 4A, S15, and S16).²⁵ The distance between metal atoms on the top layer in PdCu-BCC is longer than that in PdCu-FCC, which coincides with AC-STEM characterizations. It has been reported that the adsorption modes of HMF were highly sensitive to the microstructure of catalytic surfaces, and it further determined reactants' transformation.²⁶ Two kinds of adsorption configuration, η adsorptions and σ adsorptions, as noted in Figures 4B and 4C, were under discussion in our calculations. The interaction of HMF with PdCu surface involves the η -adsorption modes mainly via the oxygenated pendant functions (aldehyde and hydroxyl groups), while, in σ -adsorption mode, the furan ring lies flat on nanoalloy surfaces, as shown in Figure 4C. It is worth noting that dissociated adsorption modes were not taken into comparison. Besides the reactant HMF and the product DMF, the adsorptions of DHMF and MFA as key intermediates during hydrodeoxygenation were explored and the most stable adsorption structures are presented in Figures S17–S20.

HMF adsorbed on BCC (111) and FCC (100) surfaces via σ -adsorption modes with -1.00 eV and -0.71 eV, respectively, both of which were stronger than corresponding η -adsorption modes in Figure S17. Although both furan ring and aldehyde group in HMF were activated in σ -adsorption mode, either on PdCu-BCC or -FCC, the aldehyde group was first hydrogenated to produce DHMF in our experiment. This is also consistent with the results reported in the literature.^{17,18} A discussion of the reaction path of HMF hydrogenation and hydrodeoxygenation over PdCu-BCC below further demonstrates this in theory. When DHMF adsorbed on the same PdCu-BCC surface, the η configuration was favored, and the furan ring was not activated in η adsorption of DHMF. While on PdCu-FCC, DHMF preferred to be adsorbed in σ -adsorption configuration, 0.43 eV stronger than its η adsorption. The furan ring was activated in σ adsorption on FCC (100), due to the formation of new metal-carbon bonds and the partial rehybridization of ring carbon atoms from sp² to sp³, which had been reported wildly.^{17,27,28} The present chemical interactions between furan rings and FCC (100) surfaces promoted the ring hydrogenations and explained the ring reactivity of PdCu-FCC. The adsorptions of MFA and DMF were also explored both on PdCu-FCC and -BCC, and the results were similar to that of DHMF. MFA σ adsorption with ring activation was favored on PdCu-FCC, yet on PdCu-BCC the ring activation was inhibited by η adsorption (Figure S19). DMF, precluding oxygenated pendant functions, adsorbed on PdCu-BCC (100) surface weakly (-0.33 eV adsorption energy), then the furan ring remained intact. The furan ring in DMF was activated and vulnerable to hydrogenation in σ adsorption on FCC (100) with -0.45 eV adsorption energy. Thus, different ring hydrogenation reactivity over PdCu-FCC and PdCu-BCC could be attributed to the different adsorption behaviors of furan rings on these surfaces with corresponding adsorption sites.

The reaction pathway of HMF hydrogenation and hydrodeoxygenation over PdCu-BCC was also confirmed with DFT computations (Figures 5, S22, and S23). The H₂ dissociation barrier was calculated as about 0.2 eV (Figure S21), consistent with previous calculations.²⁹ Due to the low H₂ dissociation barrier, in the following steps the hydrogen atoms were assumed to adsorb on the surface directly. Hydrogenation of the carbonyl group first takes place on the C atom,

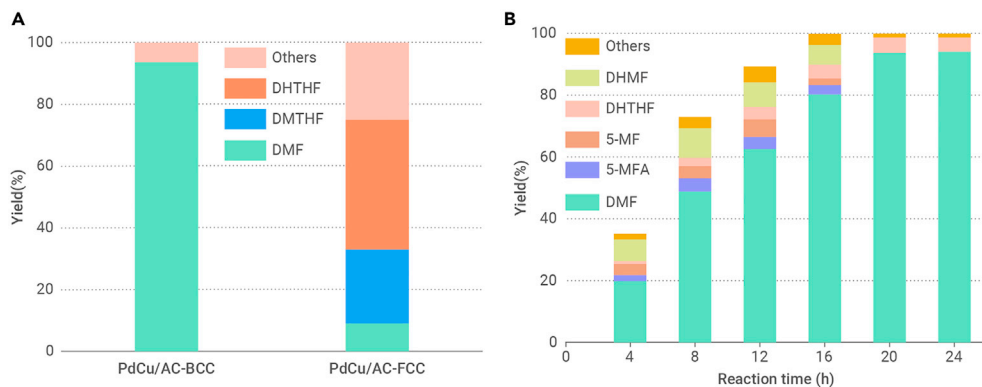


Figure 3. Catalytic performance of PdCu/AC (A) The performances of PdCu/AC-BCC and PdCu/AC-FCC for HMF hydrodeoxygenation to DMF, reaction time (20 h). (B) The effect of time on the reaction on PdCu/AC-BCC. Reaction conditions: HMF (0.3 mmol), catalyst (30 mg), solvent (THF 2 mL), reaction temperature (30°C), H₂ pressure (4 MPa), stirring speed (600 rpm).

leading to an alkoxide intermediate IM1. Next, a second hydrogen atom was added to IM1 and yielded DHMF. The overall barrier of C=O hydrogenation was 0.47 eV, then the overall barriers of hydrodeoxygenation and ring hydrogenation were calculated as 0.56 eV and 0.80 eV, indicating that the first step of HMF conversion on PdCu-BCC was hydrogenation of the carbonyl group (Figures S22 and S23). Three transition states (TS3–TS5) were confirmed during the subsequent hydrodeoxygenation of DHMF to MFA. The C–O bond scission took place over a Cu–Pd site, and the formed intermediate IM2 and OH adsorbed on sublayer Pd and top Cu, where a -0.07 eV reaction energy and a 0.95 eV barrier was calculated. One H₂O molecule was later produced from co-adsorbed OH and H, with an exothermic 0.52 eV reaction energy and a 0.46 eV barrier. After the H₂O desorption, MFA was formed through the combination of IM2 and another surface H species, which exhibited an exothermic 0.62 eV reaction energy and a 0.48 eV barrier. A similar hydrodeoxygenation pathway from MFA to DMF was calculated with an overall reaction barrier 0.89 eV and exothermic energy 1.62 eV.

The loose arrangement of surface atoms with PdCu-BCC repelled furan rings of hydrogenation intermediates, while ring adsorptions were favored by close-packing PdCu-FCC surfaces. Our work opened a new insight into the selective hydrogenation of biomass-derived furanics catalyzed by bimetallic nanoparticles. We also investigated the hydrodeoxygenation of other aromatic alcohols, and the results are presented in Table S6. PdCu/AC-BCC could catalyze the hydrodeoxygenation of a series of substrates under mild conditions with high conversions and excellent selectivities to the desired products with the aromatic rings intact.

The recyclability of PdCu/AC-BCC catalyst was evaluated at 100°C and the activity of the catalyst slightly decreased after recycling four times (Figure S14). As shown in Figure S3, the average diameter of PdCu/AC-BCC after reaction was 5.0 nm, which is similar to the fresh PdCu/AC-BCC catalyst, thus no significant sintering was observed. Also, EDS mapping shows no segregation of Pd or Cu after reactions (Figure S4). The crystallographic phase was characterized by high-resolution TEM (HRTEM), and the d-spacing of PdCu nanoalloys after reaction was 2.14 Å, corresponding to PdCu-BCC (111) facets, which means that the BCC phase of PdCu was not changed after reaction. Maybe the decrease in catalyst activity is attributed to the inevitable loss of catalyst in the recovery process, since only 16 mg of PdCu/AC-BCC (80% of the original amount) was recovered

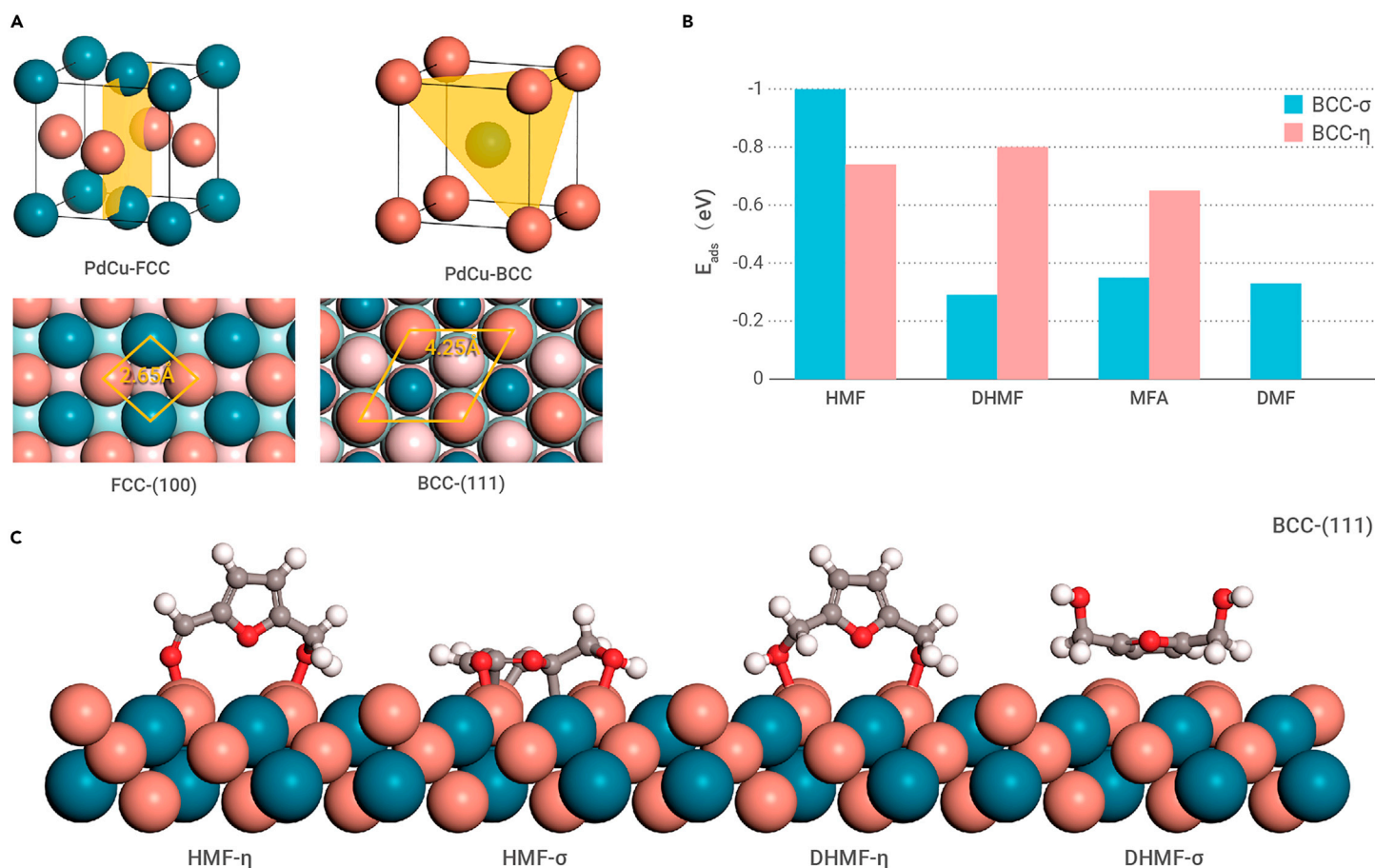


Figure 4. Furanics adsorption behaviors on PdCu surfaces (A) Exposed surfaces of PdCu-FCC/BCC considered in DFT calculations. The distances between neighbor top metal atoms are marked. (B) Adsorption energies of HMF, DHMF, MFA, and DMF on PdCu-BCC, respectively. (C) Optimized geometries for adsorption configuration of HMF and DHMF on PdCu-BCC. Dark blue, Pd; light blue, sublayer Pd; orange, Cu; pink, sublayer Cu; silver, H; gray, C; red, O.

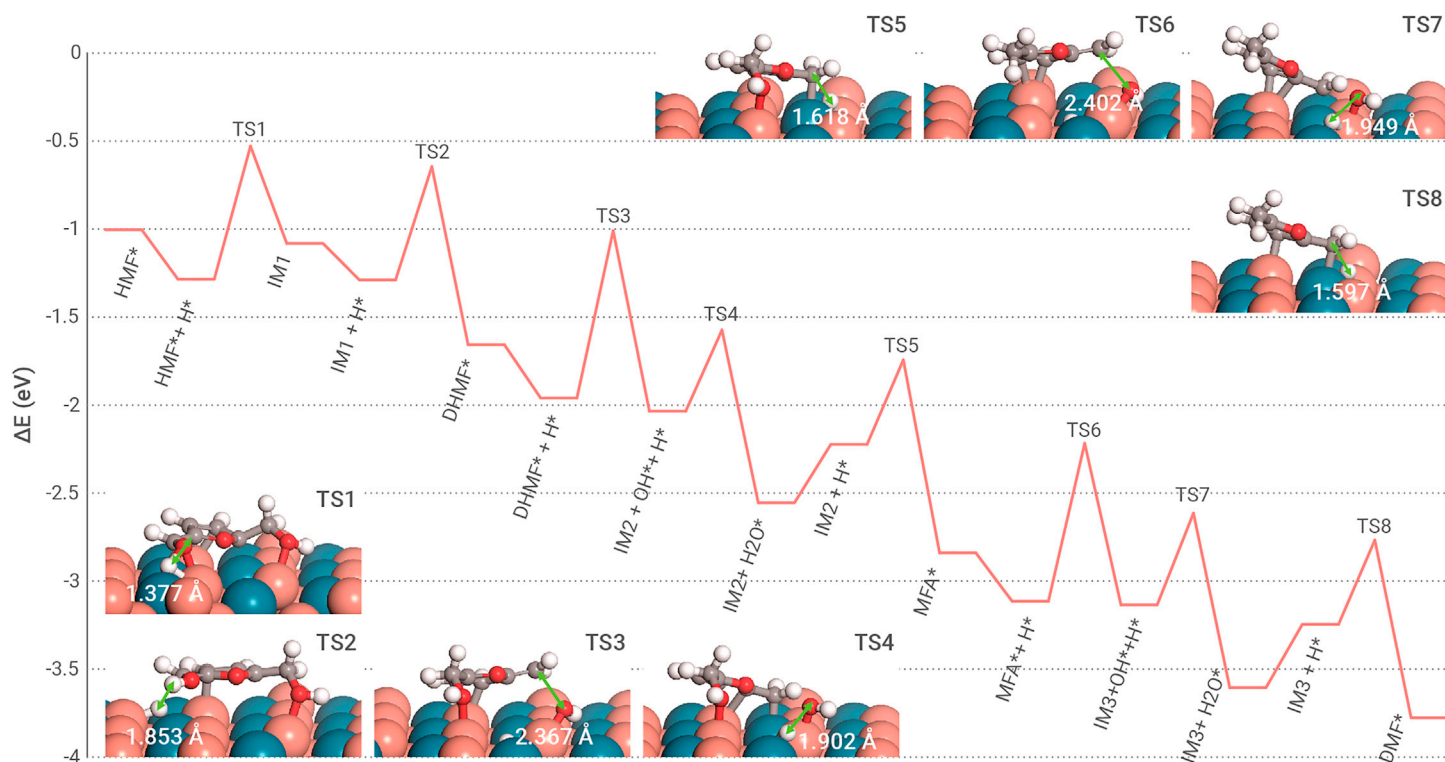


Figure 5. Reaction pathway from HMF to DMF on PdCu-BCC (111) The structures of transition states are shown in insets, in which the key atomic distances are labeled in angstroms. Dark blue, Pd; orange, Cu; silver, H; gray, C; red, O.

after the fourth run. It can be proved that the yield of the product was nearly the same as that of the first run when 0.24 mmol of HMF (80% of the amount of the first run) was added in the fifth run.

DISCUSSION

In summary, we reported that the introduction of Cu into Pd could tune the electronic structure of Pd through the electron transfer from Cu to Pd. This electronic structure feature greatly promoted the catalytic activity of PdCu nanoalloys for the hydrodeoxygenation of HMF at room temperature. The crystallographic phase of PdCu nanoalloys had a significant impact on their selectivity in the hydrogenation of HMF. On PdCu/AC-BCC, a 93.6% yield toward the desired DMF product could be reached even at room temperature. The lower energy barrier of hydrodeoxygenation of C–OH and C=O than that of furan hydrogenation over PdCu/AC-BCC resulted in the high selectivity of DMF. However, PdCu/AC-FCC preferred to promote the hydrogenation of furan ring with low DMF selectivity. We believe that the PdCu/AC-BCC catalyst has great potential for applications due to its obvious advantages, such as extremely high activity and selectivity, and being easy to prepare. In addition, the findings of this work are useful for designing other efficient catalysts for selective hydrogenation of compounds with two or more unsaturated bonds.

MATERIALS AND METHODS

Materials

CuCl₂·2H₂O (>99.0%), PdCl₂ (>99.0%), sodium borohydride, and ethyl alcohol were purchased from Sinopharm Chemical Reagent. The AC was purchased from Fujian Xinsen Chemical Industry. Tetrahydrofuran, 5-hydroxymethylfurfural, 2,5-dimethylfuran, 2,5-bis(hydroxymethyl)furan, 2,5-bis(hydroxymethyl)tetrahydrofuran, 5-methylfurfural, 5-methylfurfurylalcohol, 5-methyltetrahydrofuran-2-methanol, 2-hexanol, 2,5-dimethyltetrahydrofuran, and n-decane were purchased from J&K. H₂ (>99.99%) and Ar (>99.99%) were supplied by Beijing Analytical Instrument Company. Ultrapure water (resistivity ≥ 18 MΩ cm) was used during the experimental process.

Methods

The PdCu/AC catalysts were synthesized via the co-reduction method and were then annealed at a controlled temperature. In a typical experiment, 0.2 g of AC was dispersed in 50 mL of ultrapure water with sonication for 3 h to get a well-dispersed AC suspension.

Then, 5.0 mL of aqueous solution containing CuCl₂ and H₂PdCl₄ (with molar ratio of Cu²⁺:Pd²⁺ = 1:1) was mixed with AC suspension in an ice water bath. Then fresh aqueous solution containing NaBH₄ was added drop-wise with continuous magnetic stirring under argon atmosphere, and the reaction solution was kept stirring for 3 h to complete the reduction reaction. The obtained black granules were collected by centrifuging and washing with ultrapure water three times (3 × 30 mL) and ethanol twice (2 × 30 mL) and dried in a vacuum oven at 60°C for 12 h. The ground powder was calcined in a tube furnace (Anhui Kemi Machinery Technology, model TFV-1200-50-I-220) for 4 h (reducing gas contains 10 vol % hydrogen and 90 vol % argon) to obtain PdCu/AC. The PdCu/AC-FCC and PdCu/AC-BCC were obtained at annealing temperatures of 200°C and 400°C, respectively. The synthetic conditions for Pd/AC and Cu/AC were similar to those of PdCu/AC-BCC except for changing the ratio of Pd²⁺:Cu²⁺. PdCu/TiO₂ and PdCu/Al₂O₃ were synthesis with the same method as PdCu/AC-BCC.

Characterization

The TEM and EDS images of the catalysts were obtained using a JEOL-2100F and JEM-200F electron microscope operated at 200 kV. JEM ARM300F equipped with an EDX detector (JEOL) and an energy filter (GATAN) operated at 300 kV was used for aberration-corrected HAADF-STEM images. The XPS measurements were carried out on an ESCALAB 220i-XL spectrometer at a pressure of ~3 × 10⁻⁹ mbar (1 mbar = 100 Pa) using Al Kα as the excitation source (hν = 1,486.6 eV) and operated at 15 kV and 20 mA. The binding energies were calibrated with the C1s level of adventitious carbon at 284.8 eV as the internal standard reference. The XPS samples were prepared without exposure to the air. The XRD experiment was performed on Rigaku D/max 2500 with nickel filtered Cu-Kα (λ = 0.154 nm) operated at 40 kV and 20 mA. The contents of different elements in the PdCu/AC catalysts were analyzed by ICP-AES.

REFERENCES

- Binder, J.B., and Raines, R.T. (2009). Simple chemical transformation of lignocellulosic biomass into furans for fuels and chemicals. *J. Am. Chem. Soc.* **131**, 1979–1985.
- Huber, G.W., Iborra, S., and Corma, A. (2006). Synthesis of transportation fuels from biomass: chemistry, catalysts, and engineering. *Chem. Rev.* **106**, 4044–4098.
- Roman-Leshkov, Y., Chheda, J.N., and Dumesic, J.A. (2006). Phase modifiers promote efficient production of hydroxymethylfurfural from fructose. *Science* **312**, 1933–1937.
- Li, S., Dong, M., Yang, J., et al. (2021). Selective hydrogenation of 5-(hydroxymethyl) furfural to 5-methylfurfural over single atomic metals anchored on Nb₂O₅. *Nat. Commun.* **12**, 584.
- Nielsen, M., Alberico, E., Baumann, W., et al. (2013). Low-temperature aqueous-phase methanol dehydrogenation to hydrogen and carbon dioxide. *Nature* **495**, 85–89.

6. Yang, D., Zhu, Q., and Han, B. (2020). Electroreduction of CO₂ in ionic liquid-based electrolytes. *The Innovation* **1**, 100016. <https://doi.org/10.1016/j.xinn.2020.100016>.
7. Priece, P., Endot, N.A., Cara, P.D., and Lopez-Sanchez, J.A. (2018). Fast catalytic hydrogenation of 2,5-hydroxymethylfurfural to 2,5-dimethylfuran with ruthenium on carbon nanotubes. *Ind. Eng. Chem. Res.* **57**, 1991–2002.
8. Thananattananachon, T., and Rauchfuss, T.B. (2010). Efficient production of the liquid fuel 2,5-dimethylfuran from fructose using formic acid as a reagent. *Angew. Chem. Int. Ed.* **49**, 6616–6618.
9. Qian, Y., Zhu, L.F., Wang, Y., and Lu, X.C. (2015). Recent progress in the development of bio-fuel 2,5-dimethylfuran. *Renew. Sust. Energ. Rev.* **41**, 633–646.
10. Hansen, T.S., Barta, K., Anastas, P.T., et al. (2012). One-pot reduction of 5-hydroxymethylfurfural via hydrogen transfer from supercritical methanol. *Green. Chem.* **14**, 2457–2461.
11. Yang, P.P., Cui, Q.Q., Zu, Y.H., et al. (2015). Catalytic production of 2,5-dimethylfuran from 5-hydroxymethylfurfural over Ni/Co₃O₄ catalyst. *Catal. Commun.* **66**, 55–59.
12. Wang, X.F., Liang, X.H., Li, J.M., and Li, Q.B. (2019). Catalytic hydrogenolysis of biomass-derived 5-hydroxymethylfurfural to biofuel 2, 5-dimethylfuran. *Appl. Catal. A* **576**, 85–95.
13. Roman-Leshkov, Y., Barrett, C.J., Liu, Z.Y., and Dumesic, J.A. (2007). Production of dimethylfuran for liquid fuels from biomass-derived carbohydrates. *Nature* **447**, 982–985.
14. Luo, J., Monai, M., Wang, C., et al. (2017). Unraveling the surface state and composition of highly selective nanocrystalline Ni-Cu alloy catalysts for hydrodeoxygenation of HMF. *Catal. Sci. Technol.* **7**, 1735–1743.
15. Wang, G.H., Hilgert, J., Richter, F.H., et al. (2014). Platinum-cobalt bimetallic nanoparticles in hollow carbon nanospheres for hydrogenolysis of 5-hydroxymethylfurfural. *Nat. Mater.* **13**, 294–301.
16. Gan, T., Liu, Y.F., He, Q., et al. (2020). Facile synthesis of kilogram-scale Co-alloyed Pt single-atom catalysts via ball milling for hydrodeoxygenation of 5-hydroxymethylfurfural. *ACS Sustain. Chem. Eng.* **8**, 8692–8699.
17. Luo, J., Yun, H., Mironenko, A.V., et al. (2016). Mechanisms for high selectivity in the hydrodeoxygenation of 5-hydroxymethylfurfural over PtCo nanocrystals. *ACS Catal.* **6**, 4095–4104.
18. Guo, W.W., Liu, H.Y., Zhang, S.Q., et al. (2016). Efficient hydrogenolysis of 5-hydroxymethylfurfural to 2,5-dimethylfuran over a cobalt and copper bimetallic catalyst on N-graphene-modified Al₂O₃. *Green. Chem.* **18**, 6222–6228.
19. Wang, Q., Feng, J.T., Zheng, L.R., et al. (2020). Interfacial structure-determined reaction pathway and selectivity for 5-(hydroxymethyl)furfural hydrogenation over Cu-based catalysts. *ACS Catal.* **10**, 1353–1365.
20. Mhadmhan, S., Franco, A., Pineda, A., et al. (2019). Continuous flow selective hydrogenation of 5-hydroxymethylfurfural to 2,5-dimethylfuran using highly active and stable Cu–Pd/reduced graphene oxide. *ACS Sustain. Chem. Eng.* **7**, 14210–14216.
21. Nishimura, S., Ikeda, N., and Ebitani, K. (2014). Selective hydrogenation of biomass-derived 5-hydroxymethylfurfural (HMF) to 2,5-dimethylfuran (DMF) under atmospheric hydrogen pressure over carbon supported PdAu bimetallic catalyst. *Catal. Today* **232**, 89–98.
22. Wang, C.Y., Chen, D.P., Sang, X.H., et al. (2016). Size-dependent disorder-order transformation in the synthesis of monodisperse Intermetallic PdCu nanocatalysts. *ACS Nano* **10**, 6345–6353.
23. Ma, S., Sadakiyo, M., Heima, M., et al. (2017). Electroreduction of carbon dioxide to hydrocarbons using bimetallic Cu-Pd catalysts with different mixing patterns. *J. Am. Chem. Soc.* **139**, 47–50.
24. Biesinger, M.C. (2017). Advanced analysis of copper X-ray photoelectron spectra. *Surf. Interface Anal.* **49**, 1325–1334.
25. Zhang, R.G., Yang, M., Peng, M., et al. (2019). Understanding the role of Pd:Cu ratio, surface and electronic structures in Pd-Cu alloy material applied in direct formic acid fuel cells. *Appl. Surf. Sci.* **465**, 730–739.
26. Chen, S., Wojcieszak, R., Dumeignil, F., et al. (2018). How catalysts and experimental conditions determine the selective hydroconversion of furfural and 5-hydroxymethylfurfural. *Chem. Rev.* **118**, 11023–11117.
27. Wang, S.G., Vorotnikov, V., and Vlachos, D.G. (2014). A DFT study of furan hydrogenation and ring opening on Pd(111). *Green. Chem.* **16**, 736–747.
28. Taylor, M.J., Jiang, L., Reichert, J., et al. (2017). Catalytic hydrogenation and hydrodeoxygenation of furfural over Pt(111): a model system for the rational design and operation of practical biomass conversion catalysts. *J. Phys. Chem. C* **121**, 8490–8497.
29. Liu, L.C., Gong, H.R., Zhou, S.F., and Gong, X. (2019). Adsorption, diffusion, and permeation of hydrogen at PdCu surfaces. *J. Membr. Sci.* **588**, 117206.

ACKNOWLEDGMENTS

This work was supported by the National Natural Science Foundation of China (21871277, 22003069, 21725301, 21932002), National Key Research and Development Program of China (2017YFB0602200), and Beijing Municipal Science & Technology Commission (Z191100007219009).

AUTHOR CONTRIBUTIONS

B.H., H.L., and D.M. conceived the idea and designed research. M.D. performed the DFT calculations. S.L. synthesized the catalysts and conducted the reaction tests. M.P. performed the XPS experiments. Q.M., Y.W., J.Y., Y.Y., B.C., and S.L. performed certain experiments, and discussed and analyzed data. S.L., M.D., D.X., D.M., and H.L. wrote the paper. All authors discussed the results and commented on the paper.

DECLARATION OF INTERESTS

The authors declare no competing interests.

LEAD CONTACT WEBSITE

<http://159.226.64.165/web/23102/home>.

SUPPLEMENTAL INFORMATION

Supplemental information can be found online at <https://doi.org/10.1016/j.xinn.2021.100189>.